ACADEMIC PRESS

Available online at www.sciencedirect.com
SCIENCE DIRECT®

Journal of Catalysis 213 (2003) 211–225

JOURNAL OF CATALYSIS

www.elsevier.com/locate/jcat

Structure sensitivity for NO dissociation on palladium and rhodium surfaces

David Loffreda, Daniel Simon, and Philippe Sautet *

Institut de Recherches sur la Catalyse, Centre National de la Recherche Scientifique, 2 Avenue Albert Einstein, F-69626 Villeurbanne cedex, France
Laboratoire de Chimie Théorique et des Matériaux Hybrides, École Normale Supérieure de Lyon, 46 Allée d'Italie, F-69364 Lyon cedex 07, France

Received 10 June 2002; revised 5 August 2002; accepted 7 September 2002

Abstract

We present a comparative density-functional theory study of the chemisorption and the dissociation of the NO molecule on the close-packed (111), the more open (100), and the stepped (511) surfaces of palladium and rhodium. The energetic and kinetic properties of the reaction pathways are reported. The structure sensitivity is correlated to the catalytic activity, which can be linked to the calculated dissociation rate constants at 300 K: Rh (100) $\geqslant$ terrace Rh (511) > step Rh (511) > step Pd (511) > Rh (111) > Pd (100) $\geqslant$ terrace Pd (511) > Pd (111). The effect of the steps on the activity is found to be clearly favorable for the Pd (511) surface and unfavorable for the Rh (511) surface. The reaction barriers are correlated to the stability of the final states and the geometries of the molecular precursor states.

Keywords: Surface; Structure sensitivity; Palladium; Rhodium; Three-way catalyst; NO; Nitrogen monoxide; Adsorption; Dissociation; Reduction; Kinetic rate; Vibration; Transition state

1. Introduction

Breaking a NO bond is a crucial process for environmental catalysis, since it is an important step in the catalytic transformation of NO into harmless molecules. In the treatment of car exhaust, several metals, rhodium, palladium, and platinum, are combined for the catalytic reduction of NO and the oxidation of CO [1–3]. The activity of these three metals in the dissociation of NO is different. Rhodium plays a key role, since it allows the dissociation of NO at low temperature, provided that the coverage of the surface by NO molecules is not too high. This dissociation is much more difficult on palladium and platinum, where only a small fraction of the molecules are dissociated at room temperature. Due to this superior behavior of rhodium for the activation of NO, this metal is usually incorporated into the catalyst, and this application represented 84% of the total western-world demand for this rare and expensive metal in 1990 [3].

Not only the nature of the metal, but also the type of surface site can be important for the molecular dissociation. It is often stated that the active sites for a catalyst are defect sites, such as steps or kinks, where the metal atoms have a lower coordination and a less saturated character. The Pd (331) [4], stepped Pd (111) [5], Pd (112) [6–9], and Pd (211) [10] surfaces present a higher activity toward dissociation than the high-density (111) surface. On the Rh (331) surface [11] the dissociation occurs on the steps and/or the defect sites. The order of activity on Rh surfaces has has been reported [12] to be Rh (100) > stepped Rh (111) > Rh (111). The authors show that step sites with (111) structure are more active than step sites with (100) structure. In the case of NO dissociation on the Ru (0001) surface, it was clearly shown from STM that the dissociation occurs at steps, since the atomic fragments are found in the vicinity of these steps [13]. This fact was rationalized by a detailed theoretical study from DFT calculations [14]. The same author studied the dissociation of NO on a stepped Pd (211) surface and an edged missing-row reconstructed Pd (311) surface [15] and also found a lower energy barrier to the dissociation at steps. This sensitivity to the precise structure of the catalytic active site seems to be a rather general concept in heterogeneous catalysis.

Our goal in this paper is to compare the pathways for NO dissociation on several surfaces of Pd and Rh from a quantum chemical description of the reaction path. Three

* Corresponding author.
E-mail address: sautet@catalyse.univ-lyon1.fr (P. Sautet).

0021-9517/02/$ – see front matter
PII: S0021-9517(02)00030-1

types of surface structures will be considered: the dense (111) face, the more open (100) surface, and a stepped surface with (100) terraces: the (511) surface.

The dissociation kinetics of NO on Rh (100) and Rh (111) surfaces have been studied in detail from temperature programmed desorption and static secondary ions mass spectrometry [16,17] or electron energy loss spectroscopy [18]. On Rh (100) the dissociation energy barrier is found to be 0.38 ± 0.03 eV (with a preexponential factor $\nu_{\mathrm{dis}} = 10^{11\pm1.0}$ s^{-1}) in the limit of zero coverage [17] and 0.46 ± 0.03 eV (with a preexponential factor $\nu_{\mathrm{dis}} = 10^{11.8\pm0.7}$ s^{-1}) at a low coverage of 0.15 ML [18], while on Rh (111) the barrier is 0.67 ± 0.06 eV (with a preexponential factor $\nu_{\mathrm{dis}} = 10^{11.0\pm1.0}$ s^{-1}) at a coverage of 0.15–0.20 ML [16]. Hence the reaction is faster on the more open (100) surface, although the barrier on the (111) face is already low. The Rh (331) stepped surface, which shows (111) terraces, is 10 times more active than the (111) surface [11]. Only a few works relate to the stepped surfaces with a (100) terrace [19,20]. When NO is adsorbed onto these surfaces at 300 K, NO dissociation takes place, as it does on the (100) surface. NO dissociation is much more difficult on the Pd surfaces. A kinetic study on a stepped Pd (111) surface shows that a small fraction of the molecules is dissociated at the step for a temperature of 400 K [5]. The estimated activation energy for NO dissociation is 1.2 eV with a preexponential factor of 4×10^{11} s^{-1}.

The chemisorption and dissociation of NO on flat and stepped Pd and flat Rh surfaces has already been the subject of previous theoretical studies, the most recent ones being in the framework of density functional theory with periodic slabs. Low-temperature molecular chemisorption has been characterized on Pd (100) [21–25], Rh (100) [21, 23–25], Pd (111) [26,27], and Rh (111) [26] and the vibrational properties have been calculated [21,22,26–28]. The chemisorption on the stepped (211) surface is shown to happen at the edge of the (111) terraces at low coverage, the (001) steps being occupied at larger exposures [29]. Recently, detailed studies of the dissociation pathways have been performed on the low-index surfaces, but also at the stepped and edged Pd surface [15,30]. The calculated energy barriers are found to be much smaller at Pd steps (1.9–2.0 eV [15,30]) and edges (2.3 eV [15]) compared to the values on Pd (111) (2.7 eV [15] or 2.27 eV [30]) and (100) surfaces (2.3 eV [15]), the dissociation taking place at the edge of the terrace. For Rh (111) a barrier of 1.5 eV is found [31]. However, the stepped Rh surfaces have never been considered.

In this paper, NO dissociation will be studied from DFT calculations on (111), (100), and (511) surfaces of Pd and Rh. This is the first time that the stepped (511) surface with (100) terraces has been addressed with calculations. The reaction pathways have been determined by a precise characterization of the transition states. Section 2 will briefly recall the calculation technique and show the model structure for the Pd and Rh (511) unit cell. The chemisorption on the flat and stepped surface will be compared in Section 3, while the dissociation pathways and the transition states will be analyzed in Section 4.

2. Methodology

2.1. Computational details

In all our calculations, the Kohn–Sham equations of density functional theory are solved with the Vienna ab initio simulation program (VASP) [32–34]. The generalized gradient approximation (GGA) of Perdew–Wang 91 has been used for the exchange–correlation functional [35]. Since spin-polarized calculation tests have been performed and showed negligible total magnetic moments for the molecular adsorption and the transition states, a spin-restricted approach was considered in the rest of the study. The one-electron wavefunctions are developed on the basis of plane waves. The electron–ion interactions are described with Vanderbilt ultrasoft pseudopotentials [36] and a tight convergence of the plane-wave expansion was obtained with a moderate cutoff of 400 eV. For the simple (100) and (111) surface, a $p(2 \times 2)$ unit cell has been chosen (cf. Figs. 1a and 1b), the slab containing four atomic layers. The transition states have been recalculated in a larger $p(4 \times 4)$ array to test the convergence to the low-coverage limit in order to minimize the influence of lateral interactions between periodic images [21]. The optimized bulk nearest-neighbor separations have been chosen: 2.8 Å for Pd and 2.72 Å for Rh slabs. The vacuum separation between periodically repeated slabs was at least 9.9 Å. The 2D Brillouin zone integrations have been performed on a $5 \times 5 \times 1$ grid for the $p(2 \times 2)$ structures and on a $2 \times 2 \times 1$ grid for the $p(4 \times 4)$ unit cells. The adsorbates were positioned on the upper side of the slab. The geometry optimizations for the minima and other stationary points of the potential energy surface include the N, O, and metal atoms in the two uppermost layers of the slab, while the two lowest metallic planes were frozen in a bulk-like geometry.

2.2. The (511) surface model

The (511) surface is formed with (100) terraces and (111) step facets. A top view is shown in Fig. 1c, with a (2×1) unit cell used for the calculation corresponding to a coverage of 1/6 ML. The slab contains three layers. The possible binding sites for NO are also indicated in Fig. 1d. Since the lateral periodicity of the terrace is broken by the step, a large number of unequivalent sites is possible; the terrace sites top (T_1 and T_2), bridge (from B_1 to B_4), threefold pseudo-hollow (from pH_1 to pH_3), fourfold hollow (H_1 and H_2), and flat (from F_1 to F_5) and the step sites (S_1 and S_2 with a NO direction perpendicular to the stair riser facet). The adsorbates have been positioned on one side of the slab only, with one layer at the surface being able to relax in geometry

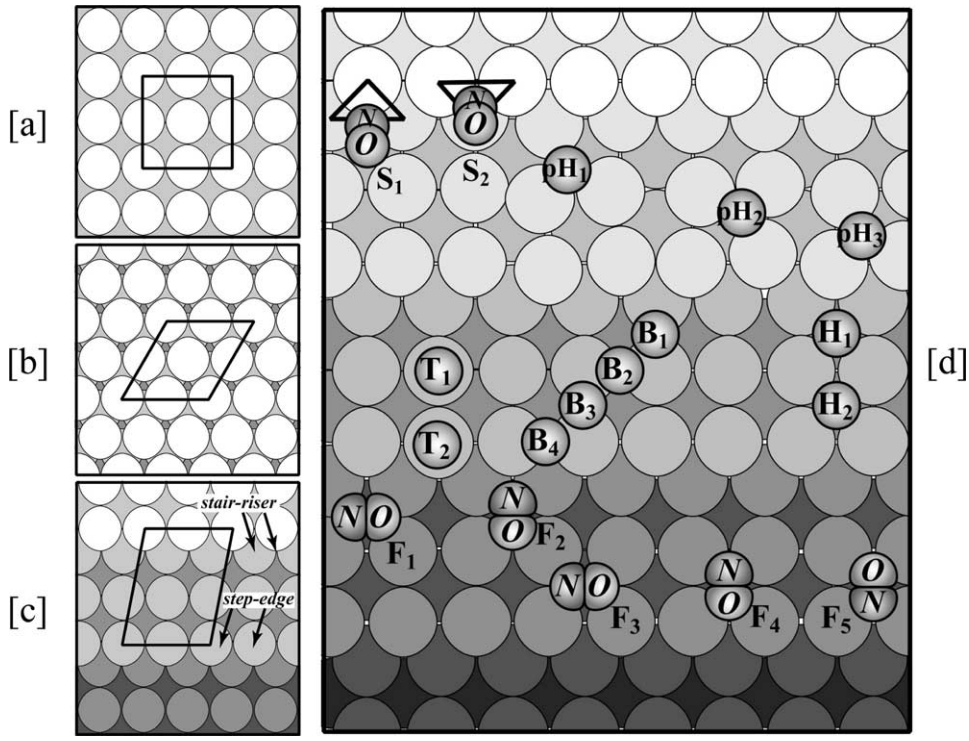

Fig. 1. Top views of the surface models [a] (100) with a $p(2 \times 2)$ unit cell, [b] (111) with a $p(2 \times 2)$ unit cell, [c] (511) with a (2×1) unit cell, and [d] (511) with the various inequivalent terrace sites, top (T_1 and T_2) , bridge (from B_1 to B_4), fourfold hollow (H_1 and H_2), threefold pseudo-hollow (from pH_1 to pH_3), flat (from F_1 to F_5), and the step sites (S_1 and S_2).

optimizations. The 2D Brillouin zone integrations have been performed on a $5\times3\times1$ grid for the (2×1) cells on both Pd and Rh (511) surfaces.

2.3. Vibrational analysis and reaction path minimization techniques

For the NO molecular adsorption states, the anharmonic stretching frequency calculation technique is based on the numerical calculation of the second derivatives of the potential energy surface. The vibrational treatment is greatly simplified by neglecting the coupling, first between the surface phonons and the N–O stretching vibrations, and second between the hard N–O stretching and the other softer bending vibrations. During the potential energy surface exploration, the metallic slab is fixed to the optimized geometry of the considered adsorption site, and the equilibrium N–O direction is also fixed. The N–O bond is stretched, keeping fixed the center of mass of the molecule. The potential energy curves are fitted with a Morse-shape potential, developed at the third order around the equilibrium state. A good accuracy for the fit of the potential is reached with a sampling of 11 equidistant calculated points in the range of ±0.05 Å around the equilibrium N–O distance. The anharmonic stretching frequency can be directly computed from the potential constants. The exact expression of the anharmonic stretching frequency (ν_{an}) can be divided into a simple harmonic frequency (ν_{ha}) and a second term which corresponds to the corrective anharmonic frequency (ν_c) [37]. The numeric error in the anharmonic frequency calculation is estimated to 8 cm^{-1} by fitting the potential with fourth-order developments of the Morse potential. So third-order equations provide good accuracy. The average value for the corrective anharmonic frequencies is 25 cm^{-1}.

The search of reaction paths and transition states has been performed using a combination of techniques: constrained optimization and the nudged elastic band method [38]. The nature of all the low-energy optimized stationary points (minima and transition states) was characterized with a numerical calculation of the Hessian matrix and a harmonic vibrational analysis, with the same degrees of freedom as in the geometry optimizations [39]. Hence one or two layers of the substrate were included in the frequency calculations. Only saddle points presenting one negative force constant will be named as transition states in the discussion. Starting from the most stable molecular adsorption state (MS), the NO dissociation generally proceeds first by a diffusion towards a metastable precursor state (PS), itself connected along the reaction path to the transition state (TS) (cf. Fig. 2). The activation energy barrier for dissociating NO (E_{act}) has been defined as the difference of the energetic stability between the transition state (TS) and the molecular precusor state (PS). When the PS is not the thermodynamic molecular state (MS), we have defined the effective activation energy barrier (E_{eff}) as the sum of E_{act} and of the diffusion energy cost between MS and PS (ΔE_{dif}). Using the vibrational information, the reaction rate constant k_{dis} for NO dissociation can then be calculated with the transition state theory in the

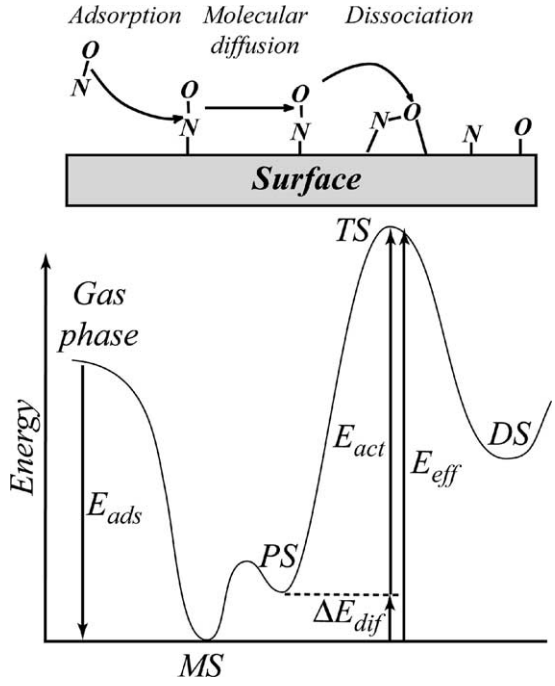

Fig. 2. Energy scheme for the NO dissociation presenting the most stable molecular adsorption state (MS), a metastable precursor state (PS), itself connected along the reaction path to the transition state (TS), and the dissociated state (DS). The dissociation activation energy barrier (E_{act}) is defined as the difference between the transition state (TS) and the molecular precusor state (PS) adsorption energies. If the PS is not the thermodynamic molecular state (MS), the effective activation energy barrier (E_{eff}) is defined as the sum of E_{act} and of the diffusion energy cost between MS and PS (ΔE_{dif}).

harmonic approach [40,41],

$$k_{\mathrm{dis}}(T) = \frac{k_{\mathrm{B}}T}{h}\frac{Q_{\mathrm{TS}}}{Q_{\mathrm{PS}}}\,\mathrm{e}^{-E_{\mathrm{act}}/(k_{\mathrm{B}}T)} = k^0\,\mathrm{e}^{-E_{\mathrm{act}}^{\mathrm{ZPE}}/(k_{\mathrm{B}}T)}, \qquad (1)$$

where Q_{TS} and Q_{PS} are the vibrational partition functions in the transition state and precursor state, respectively, E_{act} is the activation energy calculated between TS and PS, and k^0 is the preexponential factor when the activation energy is corrected for zero point energy $E_{\mathrm{act}}^{\mathrm{ZPE}}$. When PS is different from MS, there is a direct influence on the kinetics of the reaction. If we assume that the diffusion process between the molecular and the precursor states is much faster than the dissociation process then the effective reaction rate constant k_{eff} is obtained by the product of the previous rate k_{dis} and the diffusion equilibrium constant K_{dif}:

$$k_{\mathrm{eff}}(T) = K_{\mathrm{dif}}k_{\mathrm{dis}} = \mathrm{e}^{-\Delta E_{\mathrm{dif}}/(k_{\mathrm{B}}T)}k_{\mathrm{dis}} = k_0\,\mathrm{e}^{-(E_{\mathrm{act}}^{\mathrm{ZPE}}+\Delta E_{\mathrm{dif}})/(k_{\mathrm{B}}T)} = k_0\,\mathrm{e}^{-E_{\mathrm{eff}}/(k_{\mathrm{B}}T)}. \qquad (2)$$

For the kinetics of the dissociation process, the effective activation energy barrier E_{eff} has to be considered. So in the discussion, we will compare the effective activation energies E_{eff} or reaction rates k_{eff} calculated on the Pd and Rh surfaces.

3. Molecular adsorption of NO on Pd and Rh surfaces

The molecular adsorption of NO on various sites on the Pd (511) and Rh (511) surfaces is a crucial point for the study of the dissociation since the precursor states of the NO reduction are molecular chemisorbed states and they play a major role for the selection of the reaction paths. The structural, energetic and vibrational results are given in Tables 1 and 2 for the various sites (cf. Fig. 1) of Pd and Rh (511) surfaces, respectively.

For low-coverage adsorption (1/6 ML) on the palladium (511) surface, all the stable sites correspond to a vertical or slightly tilted molecular adsorption. Similarly to Pd (100) [21], no flat adsorption has been found. The gas phase NO molecule distance has been optimized to 1.174 Å with a calculated anharmonic stretching frequency of 1861 cm^{-1} (experimentally 1903 cm^{-1} [42]). The geometry optimizations show that the B_4 bridge site close to the (111) step is the most stable one with an adsorption energy of −2.34 eV (cf. Table 1 and Figs. 3 and 4a). The other terrace sites (bridge B_1, B_2, B_3, pseudo-hollow pH_1, pH_2, pH_3, and fourfold hollow H_1, H_2 sites) and step S_1, S_2 sites are also energetically favored with an adsorption energy between −1.91 and −2.27 eV (cf. Table 1). Therefore the diffusion energy barriers between all these sites should be small and the mobility of the NO molecule is high on the (100) terraces and across the (111) steps. In contrast, the top T_1, T_2 sites are not favored. For a given site family, we can infer that the strength of the adsorption increases from the stair riser to the step edge (for example, for the bridge sites from B_1 (−1.93 eV) to B_4 (−2.34 eV)). So the sites of the upper terrace near the step edge, B_4, pH_3, H_2, and the step site S_2 are the most stable ones. Previous experimental studies on the stepped Pd (112) surface (composed

Table 1
Equilibrium N–O distances $d_{\mathrm{N-O}}$ (Å), adsorption energies E_{ads} (eV), and harmonic N–O stretching frequencies ν_{ha} (cm^{-1}) and anharmonic N–O stretching frequencies ν_{an} (cm^{-1}) for the chemisorption on the Pd (511) surface with the (2 × 1)-1 NO (1/6 ML) structure

	Terrace sites											Step sites	
	Top		Bridge				Pseudo-3-fold hollow			4-fold hollow			
	T_1	T_2	B_1	B_2	B_3	B_4	pH_1	pH_2	pH_3	H_1	H_2	S_1	S_2
$d_{\mathrm{N-O}}$	1.186	1.186	1.198	1.198	1.189	1.191	1.219	1.218	1.219	1.227	1.223	1.225	1.215
E_{ads}	−1.56	−1.76	−1.93	−2.09	−2.16	−2.34	−2.03	−2.18	−2.22	−1.91	−2.13	−2.00	−2.27
ν_{ha}	1714	1726	1632	1650	1648	1641	1518	1528	1526	1446	1490	1484	1559
ν_{an}	1687	1699	1604	1623	1620	1613	1487	1497	1495	1412	1458	1452	1528

Table 2
Equilibrium N–O distances $d_{N–O}$ (Å), adsorption energies E_{ads} (eV), and harmonic N–O stretching frequencies ν_{ha} (cm^{-1}) and anharmonic N–O stretching frequencies ν_{an} (cm^{-1}) for the chemisorption on the Rh (511) surface with the $(2 \times 1) - 1$ NO (1/6 ML) structure

	Terrace sites													Step sites	
	Top		Bridge				4-fold hollow		Flat					S_1	S_2
	T_1	T_2	B_1	B_2	B_3	B_4	H_1	H_2	F_1	F_2	F_3	F_4	F_5		
$d_{N–O}$	1.181	1.186	1.210	1.205	1.205	1.203	1.247	1.234	1.338	1.313	1.308	1.323	1.310	1.237	1.227
E_{ads}	−2.08	−2.40	−2.40	−2.47	−2.55	−2.74	−2.21	−2.42	−2.10	−2.17	−2.46	−2.50	−2.60	−2.12	−2.59
ν_{ha}	1801	1774	1594	1623	1611	1614	1350	1445	893	1023	1044	969	1028	1419	1498
ν_{an}	1779	1750	1567	1594	1585	1587	1319	1412	839	971	999	919	986	1389	1468

of a flat terrace (111) and a step (001)) suggest that the NO adsorption is favored at low coverage on the terrace sites [6–9]. In contrast, for the case of Pd (511), the most stable site is found to be the near step edge bridge site B_4. Our results agree also with previous DFT calculations [30]. For the bridge site B_4 (cf. Fig. 4a) the optimal Pd–N and N–O distances are 1.96–1.97 Å and 1.191 Å, respectively. For the threefold pseudo-hollow site pH_3 (cf. Fig. 4b) the optimized Pd–N distances (2.03–2.15 Å) are inequivalent and the N–O distance (1.219 Å) is longer. For the step site S_2 (cf. Fig. 4c), the Pd–N distances are also inequivalent (2.02–2.03–2.09 Å) with a similar N–O bond length of 1.215 Å. For the fourfold hollow site H_2 both the Pd–N (2.18–2.19–2.23–2.28 Å) and the N–O (1.223 Å) distances are the longest ones. As a consequence, the Pd–N and N–O optimal bond lengths increase with the coordination degree of the site (from the twofold bridge B_4 to the fourfold hollow H_2 sites), similarly to our previous studies of NO adsorption on flat Pd and Rh (100) and (111) surfaces [21,26] and to the general trends for adsorbates on metal surfaces.

Now, let us compare the adsorption energy results for the stepped (511) surface to the flat (111) and (100) surfaces (cf. Fig. 3). First, the thermodynamic molecular state B_4 of the (511) surface is more stable than the prefered sites of the (100) and (111) surfaces, respectively the threefold pseudo-hollow site (−2.19 eV) for Pd (100) [21] and the threefold fcc hollow site (−2.29 eV) for (111) [26]. The bridge sites B_1 and B_2 (−1.93 eV and −2.09 eV, respectively) near the (111) stair riser have an energy close to that of the Pd (111) bridge site, but are less stable than the bridge site on the Pd (100) surface (−2.15 eV) [21]. However, the bridge sites B_3 and B_4 (−2.16 eV and −2.34 eV), which are close to the step edge, are more stable. The energy gain for the bridge site B_4 at the step edge is −0.19 eV with respect to the bridge position on Pd (100). For the threefold pseudo-hollow sites (−2.03, −2.18, and −2.22 eV for pH_1, pH_2, and pH_3, respectively), the trend is similar since the adsorption energy of the pseudo-hollow site on Pd (100) is −2.19 eV. The step sites S_1 and S_2 (−2.00 and −2.27 eV, respectively) can be compared to threefold sites of Pd (111): they appear to be slightly less stable on the step than on Pd (111) (−2.29 eV [26]). Likewise, the fourfold hollow sites H_1 and H_2 (−1.91 eV and −2.13 eV) are less stable than the corresponding site on Pd (100) (−2.17 eV).

For the case of the Rh (511) surface at the coverage 1/6 ML, the general trends are for the most part comparable to

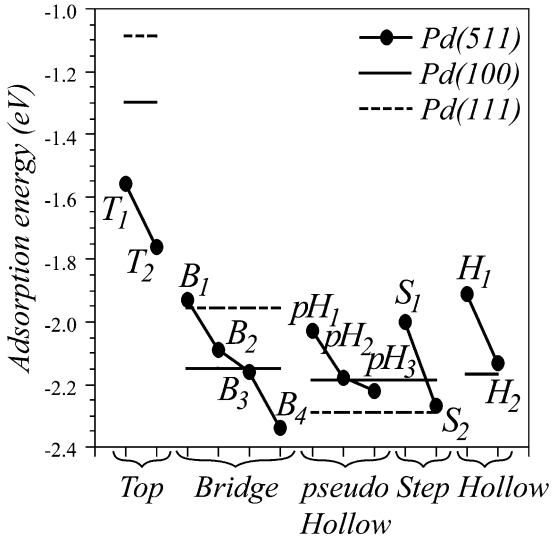

Fig. 3. Evolution with the site coordination of the adsorption energies (eV) for NO chemisorbed on the Pd (511) surface, by comparison with the Pd (100) and (111) surfaces.

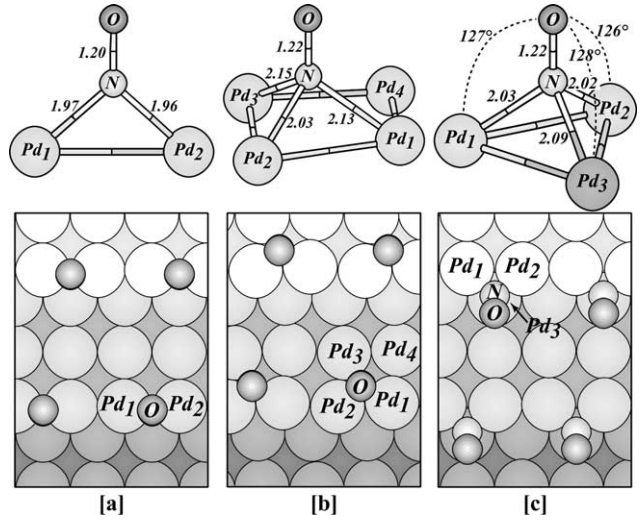

Fig. 4. Lateral and top views of the optimized geometries for the most stable sites in the case of the NO adsorption on Pd (511); [a] bridge site B_4, [b] pseudo-hollow site pH_3, and [c] hollow step site S_2. All distances are expressed in Å.

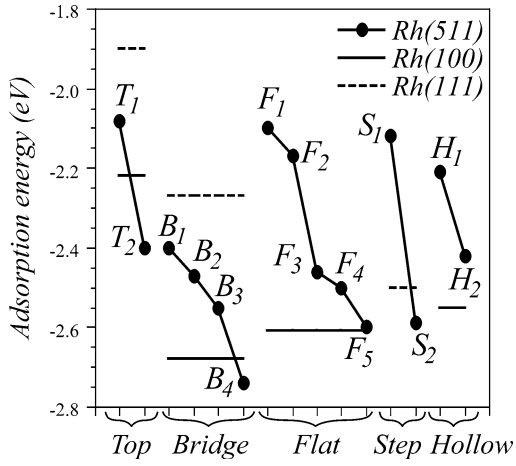

Fig. 5. Evolution with the site coordination of the adsorption energies (eV) for NO chemisorbed on the Rh (511) surface, by comparison with the Rh (100) and (111) surfaces.

the case of Pd (511) (cf. Table 2 and Fig. 5). The geometric optimizations show that the bridge site B_4 (cf. Fig. 6a) is still the most stable with an adsorption energy of −2.74 eV. However, the flat or highly inclined adsorption sites have also a good stability, similarly to the Rh (100) case [21]. The step S_2 site at the stair riser facet (−2.59 eV; cf. Fig. 6b) and the flat F_5 site (−2.60 eV; cf. Fig. 6c) are also very stable adsorption modes on this surface. The top T_2 (−2.40 eV) and fourfold hollow H_2 (−2.42 eV) sites close to the step are less favored. The same remark concerning the increased stability of the terrace sites from the stair riser to the step edge can be done for the Rh (511) surface like on Pd (511).

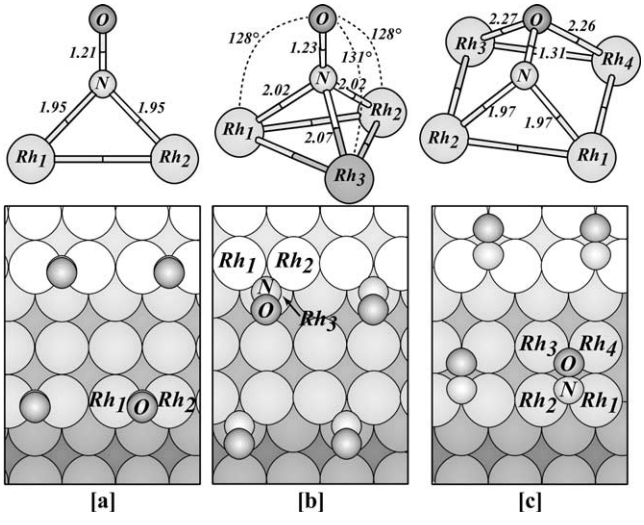

Fig. 6. Lateral and top views of the optimized geometries for the most stable sites in the case of NO adsorption on Rh (511); [a] bridge site B_4, [b] hollow step site S_2, and [c] flat site F_5. All distances are expressed in Å.

4. Dissociation pathways and transition states

The dissociation pathways of NO on the Pd and Rh (511) surfaces have been studied for a coverage of 1/6 ML in a (2×1) unit cell. Many reaction paths have been considered and we have classified them into two main families. The first family is associated with the dissociation at the stair riser facet of the Pd and Rh (511) surfaces. This family is a new one by comparison with the previous study on the flat Pd and Rh (100) surface [21]. For this new family all the dissociation pathways have been optimized in a first step with the nudged elastic band technique available in the VASP program. This method has allowed us to generate the optimized geometries of all the saddle points with a good approximation. When the residual forces on the atoms were too important in that initial guess, we have completed the minimizations by partially constrained geometry optimizations. Then in a second step, we have fully reoptimized the saddle point geometries with a quasi-Newton algorithm in order to describe them finely and proceed with the vibrational analysis and the reaction rate calculations. The second family is associated with the dissociation on the terraces of the Pd and Rh (511) surfaces. This family can be directly linked to the reaction pathways studied previously on the flat Pd and Rh (100) surfaces. As a consequence, all the considered saddle points have been built from the optimized data coming from Pd and Rh (100) for the geometrical initial guesses. As before, they have then been completely reoptimized with a quasi-Newton algorithm.

4.1. Dissociation on the steps of Pd and Rh (511)

For the exploration of the dissociation pathways on the steps of Pd (511), we have reported four different reaction paths involving the coordination of the NO molecule on the (111) step (cf. Fig. 7). Two pathways (Ps_1 and Ps_4) imply the NO dissociation with an oxygen atomic displacement going down from the (111) step facet toward the (100) terrace, and the two other pathways (Ps_2 and Ps_3) present an NO bond breaking with an oxygen displacement climbing the (111) step. In Fig. 7, two views for each reaction path have been reported for the description of the dissociation mechanism: a lateral view of the step presenting the molecular state in dashed circles for N and O atoms (the precursor state of the dissociation for each pathway) and the saddle point geometry named Ps_i (i goes from 1 to 4 for each path), and a top view of the step showing the saddle points and the corresponding initial dissociated states (not the final thermodynamic dissociated coadsorption state). The increasing index i of the state Ps_i is directly linked to the decreased energetic stability of the saddle point, as seen in Fig. 8a, where the energy profiles of the dissociation pathways have been reported with the N–O distance as reaction coordinate. In Fig. 8, the energy reference is the gas phase NO molecule and the relaxed surface slab. For Pd

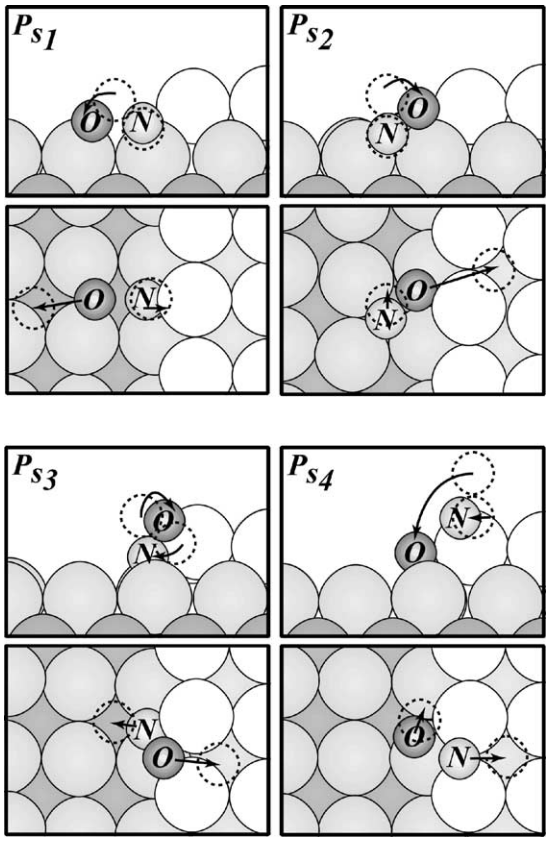

Fig. 7. Lateral and top views of the NO dissociation pathways on the step of the Pd (511) surface. The full N and O atomic spheres show the geometry of the transition state, while the initial state (respectively final state) is shown by the dashed circles in the lateral (respectively top) views. Atomic displacements between these states are sketched by the arrows. The initial molecular states are the step site S_1 for (Ps_1), the pseudo-hollow site pH_1 for (Ps_2), the step site S_2 for (Ps_3), and the bridge site B_4 for (Ps_4).

(511) (cf. Figs. 8a, 8c), the thermodynamic molecular state is the bridge site B_4 (cf. Fig. 4a) and the thermodynamic dissociated state D_P is a coadsorption state of N and O atoms, both fourfold hollow coordinated on the (100) terrace (with an adsorption energy of −1.82 eV and a N–O distance of 4.1 Å). These stationary points are respectively the initial and final states for all the reaction pathways on Pd (511) and all the effective activation energies are calculated from the bridge site B_4.

For the most favorable dissociation pathway (Ps_1), the NO molecule first diffuses from the thermodynamic site B_4 to the precursor step site S_1 (+0.34 eV) and the N–O bond breaks by tilting the molecule toward the terrace and coordinating the O atom on a bridge position. The transition state Ps_1 is the most stable one with an adsorption energy of −0.80 eV and a N–O distance of 1.91 Å. The optimized geometry is reported in Fig. 9. The N atom sits in the step hollow site with Pd–N distances of 1.94–1.97 Å, while the O atom is twofold coordinated with Pd–O distances of 2.02 Å. The N atom stays in the step hollow site during all the dissociation mechanism, while the O atom migrates to a pseudo-threefold site on the terrace close to the next step edge. The effective activation energy, 1.54 eV, is the lowest for the pathways on the steps of Pd (511). In the pathway (Ps_2), the molecular precursor state is the terrace site pH_1 (+0.31 eV less stable than B_4). The NO bond is broken by tilting the molecule towards the step and coordinating the O atom on a bridge position. In the Ps_2 state geometry, the N atom is threefold coordinated to the terrace Pd atoms of the site pH_1, while the O atom is twofold coordinated on the next step edge (the N–O distance being shortened to 1.82 Å). The effective activation energy is increased to 2.14 eV. At the end of the dissociation process, the O atom migrates from the step to a terrace threefold hollow site, while the N atom shifts from a pseudo-hollow position to the nearby fourfold hollow site. In the following pathway (Ps_3), the dissociation takes place by tilting the NO molecule on the step from the precursor state S_2. During the process the N atom is displaced from S_2 to the S_1 step site, while the O atom is positioned on a step bridge site. The N–O distance 1.85 Å is similar to that of the state Ps_2 and the effective activation energy is stronger (2.21 eV), mainly because of the greater stability of the S_2 state. Then the O atom diffuses toward the upper terrace pseudo-hollow site while the N atom diffuses in the lower terrace fourfold hollow site. For the less favorable pathway (Ps_4) (associated with the highest effective activation energy 2.56 eV), the N–O bond breaks by tilting the molecule from the precursor bridge site B_4 and coordinating the O atom on a bridge position on the (111) step. The state Ps_4 present the longest N–O distance (2.03 Å). Then the N atom diffuses toward the terrace fourfold hollow site while the O atom stays in the threefold hollow step site.

For the dissociation on the step of the Rh (511) surface, the calculated saddle points are similar to Ps_1, Ps_2, and Ps_3 obtained for the Pd (511) surface. The three explored pathways, (Rs_1), (Rs_2), and (Rs_3) have been presented in Fig. 10 and the corresponding energy profiles are reported in Fig. 8b. The thermodynamic molecular state is the bridge site B_4 (cf. Fig. 6a) and the thermodynamic dissociated state D_R is a coadsorption state of N, fourfold hollow coordinated on the terrace (100), and O, threefold hollow coordinated on the (111) step (with an adsorption energy of −3.06 eV and a N–O distance of 3.65 Å). As before, the index i of the saddle point Rs_i also decreases with the stability of the state.

A first remark concerns the large stability of the thermodynamic molecular state B_4 so that the energy cost for diffusion towards possible precursor states is more important. However, compared to Pd, a new type of flat metastable precursor states can be reached (from F_1 to F_5), and from these flat sites, the NO dissociation is easy with a low barrier. The effective activation energy barrier E_{eff} combines these two opposite effects. By comparison with Pd (511), the activation energy barriers calculated from the precursor states are strongly reduced and globally the effective activation barriers are smaller.

The best dissociation pathway on the steps of Rh (511) (Rs_1) is associated with a small effective activation energy

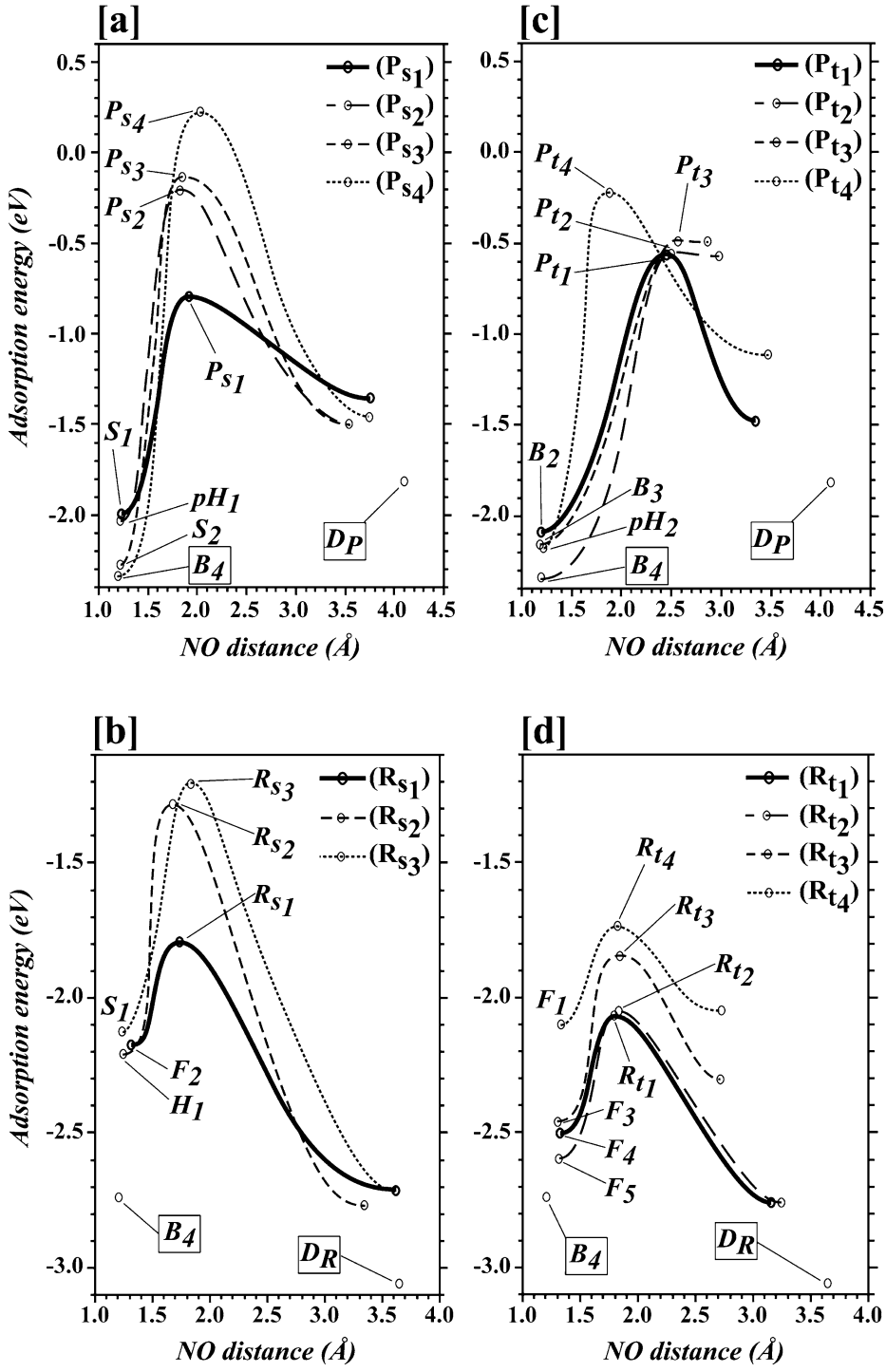

Fig. 8. Energy profiles (eV) along the N–O distance (Å) for the dissociation pathways on [a] the step of Pd (511), [b] the step of Rh (511), [c] the terrace of Pd (511), and [d] the terrace of Rh (511). The most favorable paths are presented with a bold continuous line. For all the profiles, the adsorption energies are referred to the gas phase NO molecule and the clean relaxed surface. For the Pd (511) surface, the molecular thermodynamic state is the bridge site B_4 (cf. Fig. 4a) and the final thermodynamic dissociated state is denoted D_P. For the Rh (511) surface, the molecular thermodynamic state is the bridge site B_4 (cf. Fig. 6a) and the final thermodynamic dissociated state is denoted D_R.

(0.95 eV) and a different precursor state F_2 as the pathway (Ps_1) (step site S_1). The diffusion energy cost from the molecular state B_4 to F_2 is high (+0.57 eV). As already emphasized, the existence of this new flat precursor state F_2 only stable on Rh (511) leads to an easier dissociation. Starting the reaction from S_1, the molecule diffuses to the F_2 state before beginning to dissociate. The corresponding transition state Rs_1 is the most stable one (with an adsorption energy of −1.79 eV). The optimized geometry is reported in Fig. 9. It is similar to that of Ps_1 with Rh–N distances of

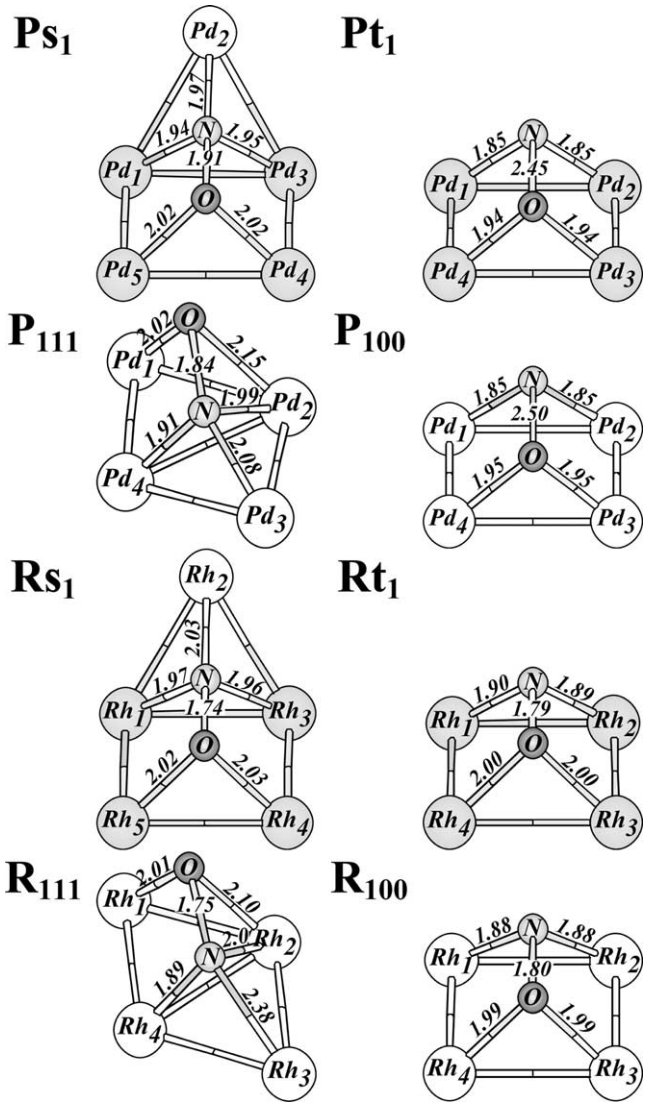

Fig. 9. Optimized geometries of the dissociation transition states: Ps_1 on the step of Pd (511), Pt_1 on the terrace of Pd (511), P_{111} on Pd (111), P_{100} on Pd (100), Rs_1 on the step of Rh (511), Rt_1 on the terrace of Rh (511), R_{111} on Rh (111), and R_{100} on Rh (100). All the distances are expressed in Å.

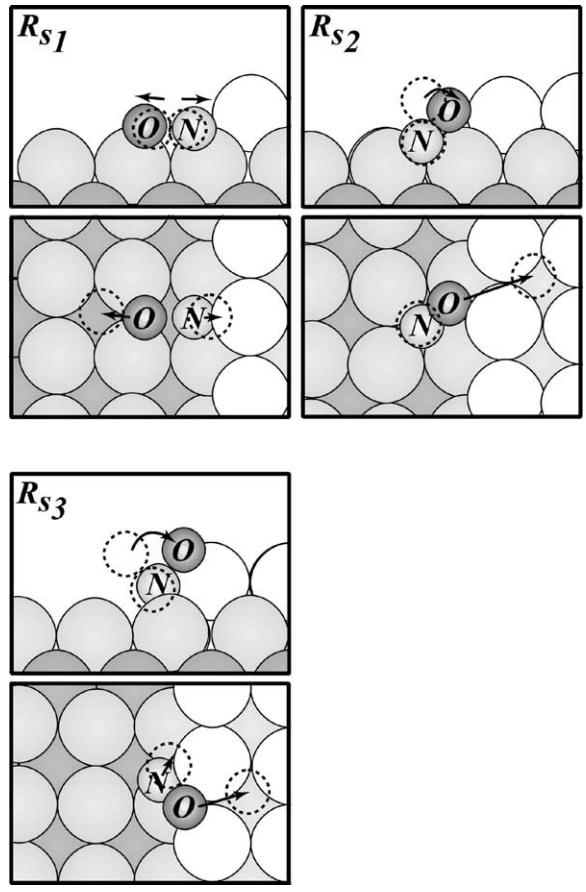

Fig. 10. Lateral and top views of the NO dissociation pathways on the step of the Rh (511) surface. The full N and O atomic spheres show the geometry of the transition state, while the initial state (respectively the final state) is shown by the dashed circles in the lateral (respectively top) views. Atomic displacements between these states are sketched by the arrows. The initial molecular states are the flat site F_2 for (Rs_1), the hollow site H_1 for (Rs_2), and the step site S_1 for (Rs_3).

1.96–2.03 Å, Rh–O distances of 2.02–2.03 Å, and a N–O distance of 1.74 Å, which is significantly shorter than for Ps_1. For the pathway (Rs_2) (that can be compared with (Ps_2)), the molecular precursor state H_1 is slightly more stable than F_2 (0.53 eV higher than B_4). The effective activation energy (1.46 eV) is higher than for (Rs_1) since Rs_2 is 0.51 eV less stable than Rs_1. However, Rs_2 is much more stable than Ps_2. For the less favorable pathway (Rs_3), the precursor molecular state is the S_1 step site and the effective activation energy is the highest one (1.54 eV). This pathway is comparable to (Ps_3) on Pd (511) with similar geometries for the Ps_3 and Rs_3 states (distance N–O of 1.83 Å). As before, the Rs_3 state is much more stable than Ps_3 for Pd (511).

4.2. Dissociation on the terraces of Pd and Rh (511)

The dissociation pathways of NO on the terrace of the Pd and Rh (511) surfaces have been strongly inspired by the reaction paths studied in the case of the Pd and Rh (100) surfaces. They are, however, significantly affected by the step since they can take place at the edge of the terrace and hence involve low coordination atoms at the step. As a consequence, the separation between step and terrace pathways is not completely clear cut. On the Pd (511) surface, four different pathways from (Pt_1) to (Pt_4) have been considered (cf. Fig. 11). The energy profiles have been reported in Fig. 8c. The best dissociation pathway (Pt_1) is associated with the molecular precursor state B_2. The diffusion energy cost between that site and the thermodynamic molecular state B_4 is 0.25 eV. The effective activation energy barrier (1.77 eV) is, however, higher than the best pathway (Ps_1) at the step. The geometry of the transition state Pt_1 (cf. Fig. 9) is similar to the Pd (100) case, but different from Ps_1, with

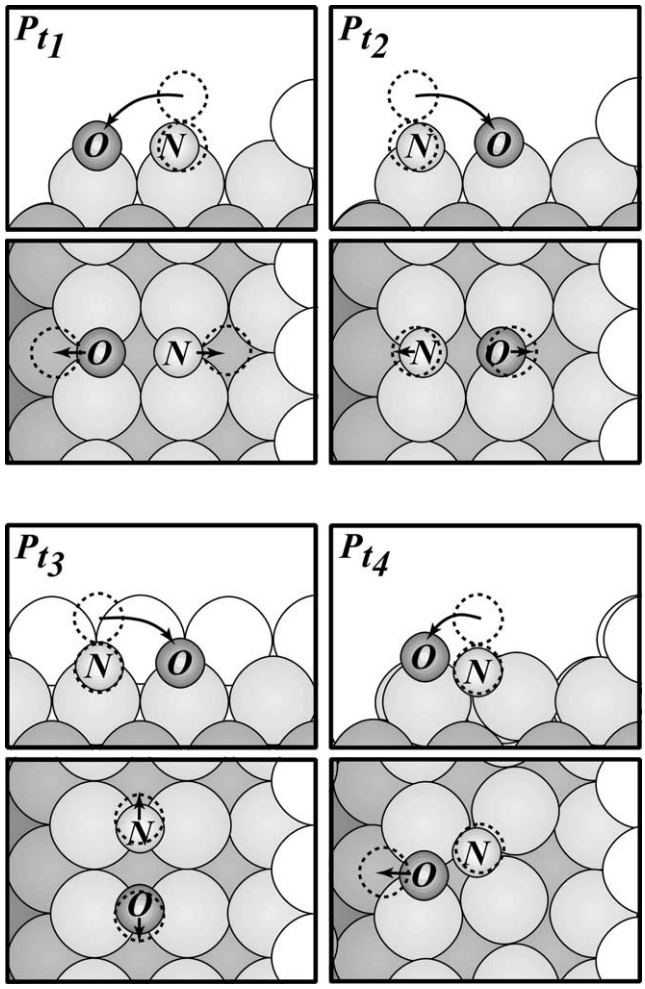

Fig. 11. Lateral and top views of the NO dissociation pathways on the terrace of the Pd (511) surface. The full N and O atomic spheres show the geometry of the transition state, while the initial state (respectively the final state) is shown by the dashed circles in the lateral (respectively top) views. Atomic displacements between these states are sketched by the arrows. The initial molecular states are the bridge site B_2 for (Pt_1), the bridge site B_4 for (Pt_2), the bridge site B_3 for (Pt_3), and the pseudo-hollow site pH_2 for (Pt_4).

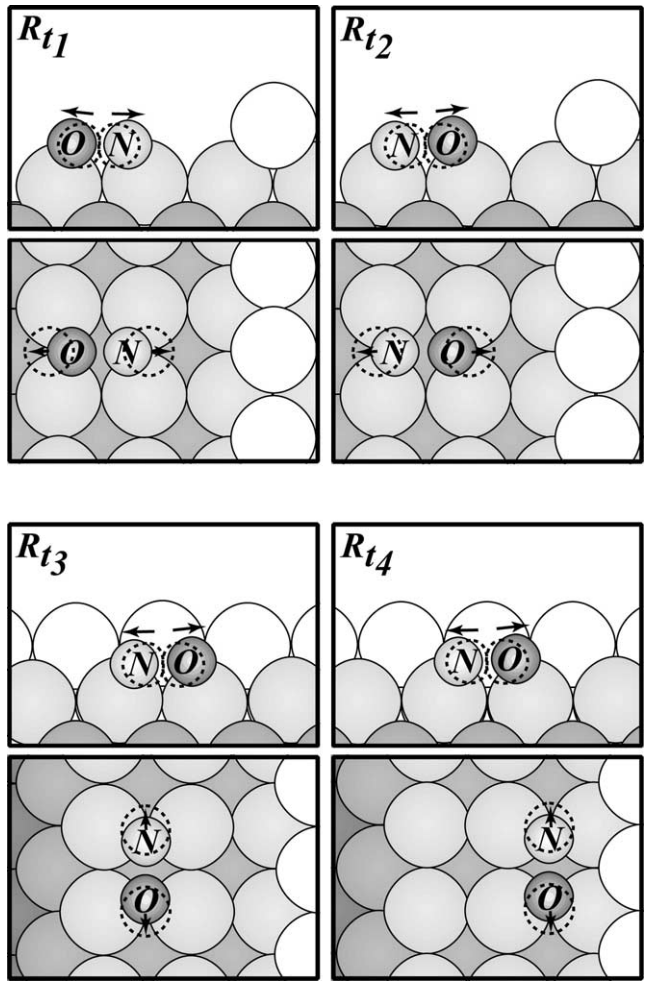

Fig. 12. Lateral and top views of the NO dissociation pathways on the terrace of the Rh (511) surface. The full N and O atomic spheres show the geometry of the transition state, while the initial state (respectively the final state) is shown by the dashed circles in the lateral (respectively top) views. Atomic displacements between these states are sketched by the arrows. The initial molecular states are the flat site F_4 for (Rt_1), the flat site F_5 for (Rt_2), the flat site F_3 for (Rt_3), and the flat site F_1 for (Rt_4).

both the N and O atoms twofold coordinated on the terrace (the O atom being coordinated with the Pd_3 and Pd_4 atoms at the step edge). The N–O distance is longer (2.45 Å) than for Ps_1 but slightly shorter than the N–O distance of 2.50 Å for the transition state on Pd (100) (cf. Fig. 9). The pathway (Pt_2) is really similar to (Pt_1), but the positions of the N and O atoms are inverted. The precursor state is B_4 and the adsorption energy of the state Pt_2 (−0.56 eV) is slightly less stable than that of Pt_1 (−0.57 eV). For the pathway (Pt_3), the N–O direction has been rotated by 90° by comparison with the cases (Pt_1) and (Pt_2). The precursor state B_3 is 0.18 eV less stable than B_4. The geometry of the state Pt_3 is really similar to that of Pt_1 and Pt_2, with a slightly elongated N–O distance of 2.57 Å, and its adsorption energy is less stable (−0.49 eV). As a consequence, the various orientations for the di-bridge-like saddle points on the hollow site at the terrace edge lead to very similar energies. All of them are clearly less stable than the Ps_1 state obtained starting from a molecule adsorbed at the stair riser facet. The last pathway (Pt_4) belongs to a different family where the precursor state is a pseudo-hollow site pH_2 and the geometry of the Pt_4 state is associated with a strong reorganization of the terrace Pd atoms with the N atom threefold coordinated and the O atom twofold coordinated. This pathway is associated with a higher effective activation energy barriers (2.12 eV) and the Pt_4 state has a shorter N–O distance (1.88 Å).

On the Rh (511) surface, four dissociation pathways have been studied and reported in Fig. 12. The corresponding energy profiles have been presented in Fig. 8d. The first three pathways, (Rt_1), (Rt_2), and (Rt_3), are associated with equivalent saddle point geometries of the three best pathways on the Pd (511) terrace, (Pt_1), (Pt_2), and (Pt_3). As already mentioned for the steps and the (100) surface, the key point for Rh compared to Pd is the existence of stable

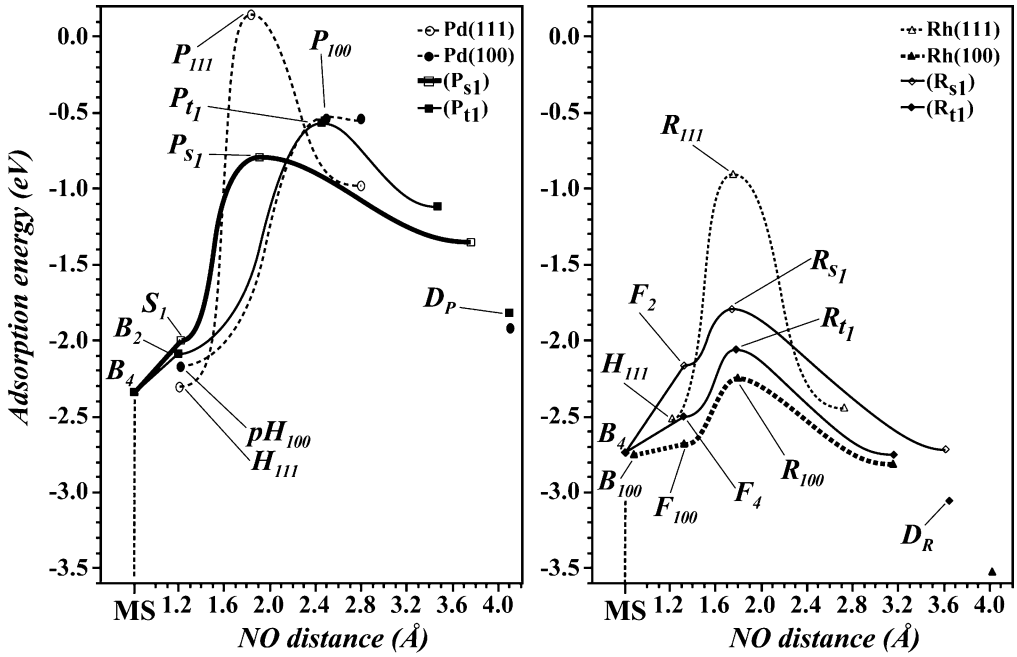

Fig. 13. Energy profiles (eV) along the N–O distance (Å) for the best dissociation pathways on the Pd (111), (100), (511) (step and terrace) surfaces and on the Rh (111), (100), (511) (step and terrace) surfaces. For all the profiles, the adsorption energies are referred to the gas phase NO molecule and the clean relaxed surface. For a purpose of visibility, the thermodynamic molecular states (MS) are shifted outside the NO distance scale on the x axis, when they are different from the corresponding precursor states.

flat precursors for NO, the N and O atoms interacting with the surface metal atoms. For the most favorable pathway (Rt_1) found on the (511) surface, the molecular precursor state is the flat site F_4, which is only 0.24 eV less stable than B_4. The transition state Rt_1 is 0.37 eV more stable than the best one at the step (Rs_1) and the effective activation energy is the weakest (0.68 eV). The geometry of Rt_1, which is reported in Fig. 9, is quite similar to that of Pt_1, at least for the coordination of the N and O atoms and their respective position on the terrace. The optimized N–O distance is, however, smaller (1.79 Å), and the Rh–N (1.89–1.90 Å) and Rh–O (2.0 Å) distances are longer. The geometry of Rt_1 is also very similar to that calculated on the Rh (100) surface (cf. Fig. 9). The following pathways are associated with various positions of such a di-bridge-like state on the terrace. The permutation of the N and O atoms yields the Rt_2 state, which is slightly less stable than Rt_1 (+0.02 eV). The two final states (Rt_3 and Rt_4), corresponding to a N–O direction parallel to the step edge, are significantly less stable than Rt_1.

4.3. Structure sensitivity and reaction constants

The structure sensitivity of the Pd and Rh surfaces toward the NO dissociation can now be studied, taking into account the best pathways found on the steps and the terraces of the Pd and Rh (511) surfaces. The open (511) surfaces have to be compared with the close-packed (100) and (111) surfaces in order to determine the influence of the surface plane on the activation energy barrier. The dissociation of the NO molecule on the Pd and Rh (100) surfaces has been studied in a previous article [21], while the dissociation on the Pd and Rh (111) is reported here (cf. Fig. 9 for the geometries of the transition states). All the optimized saddle points are true transition states, since one pure imaginary frequency has been obtained after the vibrational analysis (cf. Table 3). The best reaction pathways over all the considered surfaces of Pd and Rh (100), (111) and (511) are represented in Fig. 13. The effective activation energies and the effective dissociation rate constants at 300 K have been presented in Table 3.

For the Pd (100) case, the precursor state is the thermodynamic molecular state pH_{100} corresponding to a pseudo-hollow site. The dissociation pathway on Pd (111) is associated with a precursor state, which is the threefold fcc hollow site H_{111}. The effective activation energy barrier for Pd (100) (1.63 eV) is lower than that on the terrace of Pd (511) (1.77 eV) but higher than that at the step of Pd (511) (1.54 eV). One should notice that the activation energy difference between Pd (100) and the structurally similar terrace of Pd (511) is not related to different adsorption energies for the transition states, but to the possibility of a most stable initial state at the step edge of Pd (511). The calculated barrier for Pd (111) is the highest one (2.44 eV). These results agree with previous experimental studies [43,44]. So the best reaction pathway on Pd is found at the step of the (511) surface. This pathway (Ps_1) is associated with a lower barrier (1.54 eV) than the one proposed previously on the stepped Pd (211) surface (1.9–2.0 eV) [15,30]. This result is in better agreement with the experimental value of 1.2 eV [5]. As a consequence, the presence of low-coordinated metal

Table 3
Effective dissociation activation energies E_{eff} (eV) (including the diffusion energies between the thermodynamic and the metastable precursor molecular states), dissociation activation energies E_{act} (eV) calculated from the precursor states, N–O distances (Å) and the pure imaginary frequencies ν_{im} (cm^{-1}) for the transition states of the dissociation of NO on Pd and Rh (111), (100), and (511) surfaces

	Coverage	Activation energies		N–O distance	Imaginary frequencies	Rate constants (300 K)			
	(ML)	E_{eff} (eV)	E_{act} (eV)	(Å)	ν_{im} (cm^{-1})	$E_{\text{act}}^{\text{ZPE}}$ (eV)	k^0 (s^{-1})	k_{eff} (s^{-1})	k_{dis} (s^{-1})
P_{111}	1/4	2.44	2.44	1.84	461	2.37	7.0×10^{12}	9.8×10^{-28}	9.8×10^{-28}
P_{100}	1/16	1.63	1.63	2.50	132	1.59	6.1×10^{12}	1.0×10^{-14}	1.0×10^{-14}
Ps_1	1/6	1.54	1.20	1.91	287	1.14	6.3×10^{12}	7.7×10^{-13}	4.4×10^{-7}
Pt_1	1/6	1.77	1.52	2.45	61	1.48	6.4×10^{12}	5.3×10^{-17}	9.9×10^{-13}
R_{111}	1/4	1.61	1.61	1.75	500	1.55	5.9×10^{12}	5.6×10^{-14}	5.6×10^{-14}
R_{100}	1/16	0.50	0.44	1.80	402	0.40	6.2×10^{12}	9.1×10^{5}	1.1×10^{6}
Rs_1	1/6	0.95	0.38	1.74	418	0.35	5.8×10^{12}	2.9×10^{-3}	8.9×10^{6}
Rt_1	1/6	0.68	0.44	1.79	403	0.40	6.4×10^{12}	1.0×10^{2}	1.0×10^{6}

Each transition state is indicated with its corresponding coverage (ML) and notation; P_{111}, P_{100}, Ps_1, and Pt_1 for Pd (111), Pd (100), the step and the terrace of Pd (511), respectively, and R_{111}, R_{100}, Rs_1, and Rt_1 for Rh (111), Rh (100), the step and the terrace of Rh (511), respectively. Activation energies E_{act} corrected with zero point energy terms $E_{\text{act}}^{\text{ZPE}}$ (eV) are also reported with preexponential factors k^0 (s^{-1}), effective dissociation rate constants k_{eff} (s^{-1}) (cf. Eq. (2)), and dissociation rate constants k_{dis} (s^{-1}) at 300 K (cf. Eq. (1)).

atoms at the step on Pd (511) greatly enhances the adsorption strength of the transition state (−0.26 eV between P_{100} and Ps_1). This effect is balanced by an initial state for Pd (511) −0.17 eV more stable than for Pd (100). So the effective activation energy order on the Pd surfaces is the following: step (511) < (100) < terrace (511) < (111). The effective kinetic rate order is directly transferable (cf. Table 3). The highest effective rate constant at 300 K (7.7×10^{-13} s^{-1}) is found at the step of Pd (511), where the effective activation energy is the lowest (1.54 eV). However, the rate is very small, so this result agrees with the experiments that show a difficult NO dissociation at room temperature even on the more open Pd surfaces such as the (511) surface. For all the Pd surfaces the calculated preexponential factors are in the range 6 to 7×10^{12} s^{-1} and the zero-point energy corrections to the activation energies are weak (between 0.04 and 0.07 eV). The optimized geometries of the transition states on Pd (111) and (100) are reported in Fig. 9. For the transition state P_{111}, the N atom is threefold coordinated while the O atom is twofold coordinated and the N–O distance (1.84 Å) is shorter than those of P_{100} (2.50 Å) and Pt_1 (2.45 Å). The geometry of P_{111} can be compared to that of Ps_1 (cf. Fig. 9) and the adsorption strength of both transition states is correlated to the coordination number of the Pd atoms bonded to the N and O atoms. In fact, P_{111} is less stable than Ps_1 since the Pd_2 atom in Fig. 9 is bonded to both N and O atoms, while for Ps_1 the dissociation pathway never involves Pd atoms multicoordinated with the reactive molecule NO. This correlation has already been mentioned by Hammer [14]. Another correlation can be done between the reaction energy barrier and the coadsorption energy of the final dissociated states N + O, calculated with the reference of the NO gas phase (cf. Fig. 14) [14,21]. A linear correlation with a slope of 0.73 has been obtained. The structure sensitivity expressed by the height of the effective activation energy is directly correlated to the stability of the final thermodynamic coadsorption state. The barrier is the lowest one for the most stable final states.

For the Rh (100) case, the precursor molecular state is the flat adsorption site F_{100}, while the thermodynamic state is the bridge site B_{100}. The calculated effective activation energy (0.50 eV) is the lowest one for all the Pd and Rh surfaces (cf. Table 3). This value clearly agrees with the experimental one (0.46 ± 0.03 eV [18]). The reaction pathway on Rh (111), which has a precursor state threefold hcp hollow site H_{111}, is associated with the highest activation barrier on the Rh surfaces (1.61 eV). This value is, however, significantly higher than the experimental one (0.67 ± 0.06 eV) [16]. Nevertheless, the transition state R_{111}

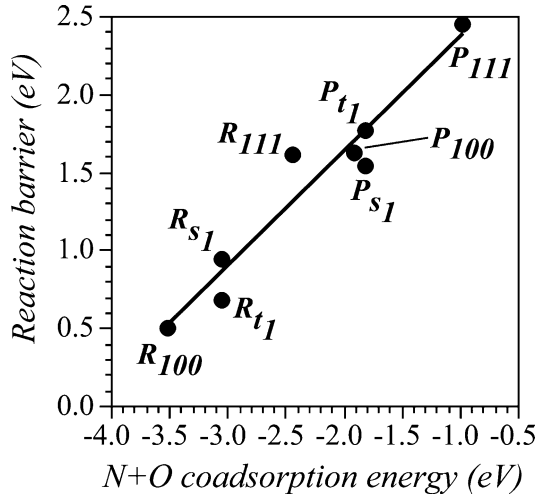

Fig. 14. Correlation diagram between the reaction activation energy barrier (eV) and the coadsorption energy of the final dissociated state (eV) referred to the gas phase NO molecule, for the dissociation pathways calculated on the Pd and Rh (111), (100), (511) (step and terrace) surfaces. P_{111}, P_{100}, Ps_1, and Pt_1 refer respectively to Pd (111), Pd (100), the step and the terrace of Pd (511), and R_{111}, R_{100}, Rs_1, and Rt_1 refer respectively to Rh (111), Rh (100), the step and the terrace of Rh (511).

is the only saddle point obtained on the Rh (111) surface (the di-bridge-like position was not found to be a stationary point). The dissociations on the step (0.95 eV) and the terrace (0.68 eV) of Rh (511) are intermediate cases between Rh (100) and (111) (cf. Fig. 13). Hence, in contrast to the Pd case, the step of Rh (511) does not enhance the adsorption strength of the transition states by comparison with the Rh (100) surface. Since the thermodynamic molecular states B_4 and B_{100} on the Rh (511) and (100), respectively, have the same stability, the main effect of the step is to destabilize the flat precursor states which are responsible for the strong activity on the Rh (100) surface. The effective activation energy order for the dissociation on the Rh surfaces is hence the following: (100) < terrace (511) < step (511) < (111). According to the experiments, the activity is strongest on Rh (100), where the effective kinetic rate constant at 300 K is the highest (9.1×10^5 s^{-1}) (cf. Table 3). On the steps of the (511) surface the activity is strongly lowered (2.9×10^{-3} s^{-1}). The discrepancy between experiment and theory for the NO dissociation barrier on Rh (111) could be explained by the presence of steps presenting (100) type facets, and hence lowering the activation barrier. Although such stepped (111) surfaces have not been explicitly considered in this study, the presence of (100) microfacets would certainly decrease the energy barrier, leading to a value close to the terrace of the Rh (511) surface. Hence NO dissociation activity would be dominated by steps on the Rh (111) surface. The optimized geometries of the transition states R_{111} and R_{100} are given in Fig. 9. The geometry of R_{111} is similar to the one of P_{111} and the same remark can be done for the correlation with the geometry of Rs_1 (cf. Fig. 9). The correlation between the reaction energy and the coadsorption energy of the final state is also presented in Fig. 14. As discussed before for the Pd surfaces, the effective activation energy is linked to the stability of the final dissociated state for the Rh surfaces. We can see on Fig. 14 that the worst Rh surface candidate for breaking the NO bond is perfect Rh (111). However, this surface is more efficient for the dissociation than the majority of the Pd surfaces (except for the steps of Pd (511)). These results are fully compatible with the experimental observations indicating that the NO adsorption is associative on the Pd surfaces, except on the surface defects where the dissociation can occur at high temperature, while the adsorption on the Rh surfaces is mainly dissociative. It can be underlined that the calculated reaction rates are completely dominated by the variation of the activation barrier. A calculation with fixed standard preexponential factors would have led to similar results and conclusions.

5. Conclusion

The chemisorption and dissociation properties of the NO molecule have been presented within the density-functional theory on the (111), the (100), and the stepped (511) surfaces of Pd and Rh. The comparative study of the adsorption sites and of the associated N–O stretching frequencies between the Pd and Rh (511) surfaces has been addressed. The adsorption is stronger for the bridge sites at the step edge where the stretching frequency is decreased. The flat adsorption is also possible on the terraces of Rh (511), as for the Rh (100) surface. The calculations of the dissociation pathways have been reported by comparing the reaction activation energy barriers and the kinetic rate constants at room temperature. The structure sensitivity of each considered Pd or Rh surface has been correlated with the rate constant, the geometry of the dissociation precursor state and the stability of the final dissociated state. On the Pd surfaces, the activity is clearly limited at room temperature even on the steps of Pd (511), where the dissociation barrier is the lowest. The high activation energy barriers have been correlated to vertical precursor states and a weakly stable final coadsorption state. The effect of the open structure (step) on the Pd surfaces is favorable but clearly limited. On the Rh surfaces, the activity is strongly enhanced and the dissociation rate is the highest on the (100) surface. The flat molecular precursor states have a key role towards the activity. The lowest effective activation barrier has been correlated to the most stable dissociated state. This open Rh (100) surface yields a strongly reduced barrier compared to the dense Rh (111) surface. In contrast with Pd, the stepped Rh (511) surface does not lower the barrier further. On the contrary, the activity on the steps and the terraces of Rh (511) is decreased compared to the Rh (100) case, since the diffusion energy costs from the thermodynamic state to the flat precursor states are enhanced. The stability of the final state appears to be a good criteria for a correlation with the reaction barrier. This study has been focussed on the single NO dissociation step. The analysis of the complete catalysis cycle for a CO + NO reaction would require the consideration of other reaction steps, such as N_2 desorption, which could limit the overall rates for cases where the NO dissociation barrier is very small.

Appendix A. N–O stretching frequency analysis

For NO chemisorption on transition metal surfaces, the experimental assignment of the adsorption sites is generally based on the interpretation of vibrational spectra. So a detailed theoretical analysis of the N–O stretching frequencies makes it possible to check the site stability order and also to improve the assignment of the observed vibrational peaks [26]. However, in the case of the Pd and Rh (511) surfaces, the calculated frequencies cannot be compared to experiments since up to now no vibrational data on chemisorbed NO have been published for neither of the two (511) surfaces. Nevertheless a direct comparison of the frequencies can be done with previous DFT results [21,26] and experiments for the flat Pd and Rh (100) and (111)

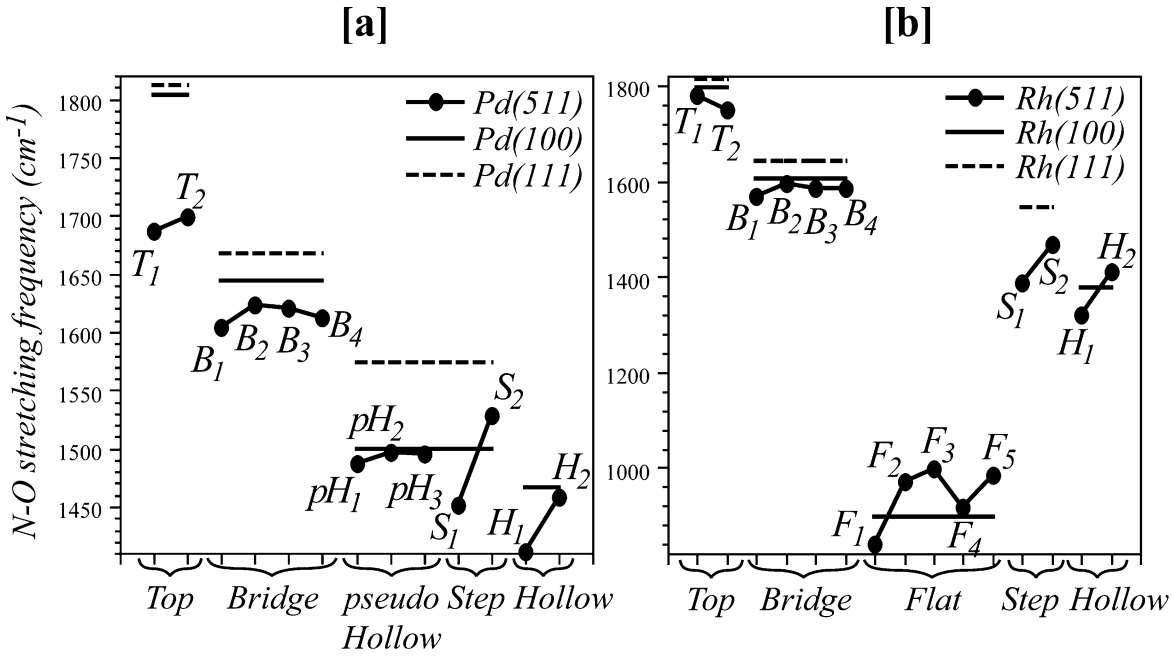

Fig. 15. Evolution with the site coordination of the N–O anharmonic stretching frequencies (cm^{-1}) for NO chemisorbed [a] on the Pd (511) surface by comparison with the Pd (100) and (111) surfaces, [b] on the Rh (511) surface by comparison with the Rh (100) and (111) surfaces.

surfaces. So these results on stepped surfaces will show how the defects can influence the N–O stretching frequency.

For the Pd (511) surface at coverage 1/6 ML, the calculated anharmonic N–O stretching frequency associated with the most stable bridge B_4 site is 1613 cm^{-1} (cf. Table 1 and Fig. 15a). For the bridge site family (from B_1 to B_4), the optimized N–O distances (1.189–1.198 Å) are close to the N–O bond length of the bridge site on Pd (100) (1.197 Å) [21]. The anharmonic frequency increases from the site B_1 to B_2 (from 1604 to 1623 cm^{-1}) then decreases from B_2 to B_4 (from 1623 to 1613 cm^{-1}). The stretching frequency of the site B_2 located in the middle of the terrace is the closest to the one calculated on Pd (100) (1644 cm^{-1}) [21]. In the case of the threefold pseudo-hollow sites pH_1 to pH_3, the optimized N–O distances (1.218–1.219 Å) are close to the bond length for the pseudo-hollow site on Pd (100) (1.219 Å) [21]. The anharmonic stretching frequency of the most stable pseudo-hollow site pH_3 is 1495 cm^{-1}. The frequency is the closest to the one of a pseudo-hollow site on Pd (100) (1499 cm^{-1}) for the pH_2 site which is located in the middle of the terrace. For the fourfold hollow sites, the stretching frequencies are weaker (1412 and 1458 cm^{-1}) than on Pd (100) (1467 cm^{-1}), while the N–O distances did not change significantly (1.227–1.223 Å). Similarly the step sites S_1 and S_2 present weaker stretching frequencies (1528 and 1452 cm^{-1}, respectively) than on the flat Pd (111) surface (1574–1588 cm^{-1} [26]). The comparison of the top sites T_1 and T_2 with the corresponding top site on Pd (100) is more delicate since on Pd (511) the NO molecule is tilted. The stretching frequencies (1687 and 1699 cm^{-1}) are found to be softer than for a vertical adsorption on Pd (100) or Pd (111) (1804 and 1812 cm^{-1} [26], respectively).

For the adsorption on Rh (511) at coverage 1/6 ML, the most stable site B_4 shows an anharmonic stretching frequency of 1587 cm^{-1} (cf. Table 2 and Fig. 15b). All the trends observed for the bridge sites on Pd (511) are still valid for the frequency analysis on Rh (511). For the bridge sites, the optimized N–O distances (1.203–1.210 Å) are close to the bond length obtained for the bridge site on Rh (100) (1.206 Å) [21]. The anharmonic stretching frequency increases from the site B_1 to B_2 (from 1567 to 1594 cm^{-1}) and then decreases from B_2 to B_3–B_4 (from 1594 to 1585–1587 cm^{-1}). For the flat sites, the situation is more complex (cf. Table 2 and Fig. 15b). The stretching frequency increases from the F_1–F_2 sites to F_3 (from 839 to 999 cm^{-1}). This frequency hardening is correlated with a shortening of the N–O bond length (from 1.338 to 1.308 Å). Then the frequency decreases to 919 cm^{-1} and the N–O distance stretches to 1.323 Å. This site present a frequency similar to that for the flat site on Rh (100) (897 cm^{-1}) and a N–O bond length of 1.329 Å [21]. Finally the frequency increases from F_4 to F_5 (919 to 986 cm^{-1}) while the NO distance shortens (from 1.323 to 1.310 Å). For the fourfold hollow sites, the optimized N–O distance is longer for H_1 (1.247 Å) by comparison with the hollow site on Rh (100) (1.236 Å) and shorter for H_2 (1.234 Å). This trend is compatible with a softer N–O stretching frequency for H_1 (1319 cm^{-1}) and a stronger frequency for H_2 (1412 cm^{-1}), since the hollow site frequency is 1378 cm^{-1} on Rh (100). This phenomenon is true also for the top sites. For the steps sites S_1 and S_2 the anharmonic stretching frequencies are weaker (1389 cm^{-1} for S_1 and 1468 cm^{-1} for S_2) than for

the fcc and hcp hollow sites on Rh (111) (1544–1554 cm^{-1} [26]). This trend is also compatible with the elongation of the N–O distances (1.237 Å for S_1 and 1.227 Å for S_2) by comparison with the hollow sites on Rh (111) (1.217 Å) [26].

References

[1] M. Shelef, G.W. Graham, Catal. Rev. Sci. Eng. 36 (1994) 433.
[2] B.E. Nieuwenhuys, Adv. Catal. 44 (1999) 259.
[3] K.C. Taylor, Catal. Rev. Sci. Eng. 35 (1993) 457.
[4] P.W. Davies, R.M. Lambert, Surf. Sci. 110 (1981) 227.
[5] H.-D. Schmick, H.-W. Wassmuth, Surf. Sci. 123 (1982) 471.
[6] R.D. Ramsier, Q. Gao, H. Neergaard Waltenburg, K.-W. Lee, O.W. Nooij, L. Lefferts, J.T. Yates Jr., Surf. Sci. 320 (1994) 209.
[7] R.D. Ramsier, Q. Gao, H. Neergaard Waltenburg, J.T. Yates Jr., J. Chem. Phys. 100 (1994) 6837.
[8] Q. Gao, R.D. Ramsier, H. Neergaard Waltenburg, J.T. Yates Jr., J. Am. Chem. Soc. 116 (1994) 3901.
[9] R.D. Ramsier, K.-W. Lee, J.T. Yates, Langmuir 11 (1995) 169.
[10] M. Ikai, K.-I. Tanaka, J. Chem. Phys. 110 (1999) 7031.
[11] L. deLouise, N. Winograd, Surf. Sci. 159 (1985) 199.
[12] R.M. Wolf, J.W. Bakker, B.E. Nieuwenhuys, Surf. Sci. 246 (1991) 135.
[13] T. Zambelli, J. Wintterlin, J. Trost, G. Ertl, Sci. 273 (1996) 1688.
[14] B. Hammer, Surf. Sci. 459 (2000) 323.
[15] B. Hammer, J. Catal. 199 (2001) 171.
[16] H.J. Borg, J.F.C.-J.M. Reijerse, R.A. van Santen, J.W. Niemantsverdriet, J. Chem. Phys. 101 (1994) 10052.
[17] M.J.P. Hopstaken, J.W. Niemantsverdriet, J. Phys. Chem. B 104 (2000) 3058.
[18] J.S. Villarrubia, W. Ho, J. Chem. Phys. 87 (1987) 750.
[19] M.F.H. Van Tol, B.E. Nieuwenhuys, Appl. Surf. Sci. 67 (1993) 188.
[20] N.M.H. Janssen, A.R. Cholach, M. Ikai, K. Tanaka, B.E. Nieuwenhuys, Surf. Sci. 382 (1997) 201.
[21] D. Loffreda, F. Delbecq, D. Simon, P. Sautet, J. Chem. Phys. 115 (2001) 8101.
[22] D. Loffreda, F. Delbecq, D. Simon, P. Sautet, J. Phys. Chem. B 105 (2001) 3027.
[23] M.-H. Tsai, K.C. Hass, Phys. Rev. B 51 (1995) 14616.
[24] K.C. Hass, M.-H. Tsai, R.V. Kasowski, Phys. Rev. B 53 (1996) 44.
[25] W. Mannstadt, A.J. Freeman, Phys. Rev. B 55 (1997) 13298.
[26] D. Loffreda, D. Simon, P. Sautet, Chem. Phys. Lett. 291 (1998) 15.
[27] K. Honkala, P. Pirilä, K. Laasonen, Surf. Sci. 489 (2001) 72.
[28] M.P. Jigato, K.S. Somasundram, V. Termath, N.C. Handy, D.A. King, Surf. Sci. 380 (1997) 83.
[29] B. Hammer, J.K. Nørskov, Phys. Rev. Lett. 79 (1997) 4441.
[30] B. Hammer, Faraday Discuss. 110 (1998) 323.
[31] M. Mavrikakis, L.B. Hansen, J.J. Mortensen, B. Hammer, J.K. Nørskov, in: D.G. Truhlar, K. Morokuma (Eds.), Transition State Modeling for Catalysis, in: ACS Symposium Series, Vol. 721, Am. Chem. Society, Washington, DC, 1999, p. 245, Chapt. 19.
[32] G. Kresse, J. Hafner, Phys. Rev. B 47 (1993) RC558.
[33] G. Kresse, J. Hafner, Phys. Rev. B 48 (1993) 13115.
[34] G. Kresse, J. Furthmüller, Phys. Rev. B 54 (1996) 11169.
[35] J.P. Perdew, Y. Wang, Phys. Rev. B 45 (1992) 13244.
[36] D. Vanderbilt, Phys. Rev. B 41 (1990) 7892.
[37] P.W. Atkins, R.S. Friedman, Molecular Quantum Mechanics, 3rd ed., Oxford University Press, Oxford, 1997.
[38] G. Mills, H. Jonsson, G.K. Schenter, Surf. Sci. 324 (1995) 305.
[39] D. Loffreda, PhD thesis, Université Claude Bernard Lyon I, France, 1999.
[40] K.J. Laidler, Theories of Chemical Reaction Rates, McGraw–Hill, New York, 1969.
[41] K.J. Laidler, Chemical Kinetics, 3rd ed., Harper Collins, New York, 1987.
[42] K. Nakamoto, Infrared and Raman Spectra of Inorganic and Coordination Compounds, 4th ed., Wiley, New York, 1986.
[43] S. Sugai, H. Watanabe, T. Kioka, H. Miki, K. Kawasaki, Surf. Sci. 259 (1991) 109.
[44] D.R. Rainer, S.M. Vesecky, M. Koranne, W.S. Oh, D.W. Goodman, J. Catal. 167 (1997) 234.